Journal of Physical Chemistry and Functional Materials (JPCFM)

journal homepage: http://dergipark.gov.tr/jphcfum

Received: 4 July 2018 Accepted: 1 August 2018 Research Article

Low-temperature Synthesis and Characterization of Bismuth Ferrite/Graphene Oxide Nano electroceramics by the Hydrothermal Method

Cihat Aydin[1*], Handan Aydin[2], Mustafa Taskin[1]

[1]*Department of Metallurgy and Materials Engineering, Faculty of Engineering, Mersin University, Mersin, Turkey.*

[2]*Department of Metallurgy and Materials Engineering, Faculty of Engineering, Munzur University, Tunceli, Turkey.*

**Corresponding Author: cihataydin_26@hotmail.com*

Abstract

Nano electroceramic samples of Bismuth Ferrite/Graphene Oxide were prepared by the hydrothermal process. The crystalline structure, morphological properties, electrical and optical properties of samples were investigated. X-ray results confirm that all the BFO nanopowders are polycrystalline with a cubic structure. The crystallite sizes and lattice parameters values of the samples were calculated. SEM and TEM results indicate that the Bismuth ferrite/Graphene oxide powders have nanostructure. The average grain size values of the powders were found to be 351, 337, 411 and 371nm for BF0, BFO20, BFO50 and BFO100 samples, respectively. The effects of the Graphene oxide doped on the Bismuth ferrite are resulted in a change of grain size. The optical band gaps of the nano electroceramics were calculated for the various amount of Graphene oxide. The optical constants of the Bismuth Ferrite were changed with Graphene oxide doping. The room temperature dielectric measurement with frequency reveals the dielectric constant and loss are affected with increasing frequency for BFO nanoceramics. The alternating current conductivity of the as-synthesized nano electroceramics increases with the increasing frequency. The obtained results suggest that the structural, optical and electrical properties of BFO can be controlled and changed by Graphene Oxide doping.

Key Words: Bismuth Ferrite; Graphene Oxide; Hummers Method; Hydrothermal Process; Nano electroceramics.

1. Introduction

Nowadays the commercial prominence in the multifunctional material industry has long been seeking a new class of highly electric, magnetic, mechanical and structural properties and design and synthesis of nanostructures for next generation, especially in the domains of Multiferroic technologies. Multiferroics are a class of which exhibit simultaneous effects of multifunctional material as they exhibit exotic properties at the nanoscale [1]. For this reason, Multiferroic is one group of electronic materials (also can be composite) with promising future [2].

Defined as a multiferroics material, BFO has attracted increasing attention because of their technological applications and some physical properties [3,4]. Bismuth ferrite is one of the very few multiferroics [5] widely known single-phase multiferroic material possessing with multiferroic behaviors such as simultaneously magnetic and electric ordering [6] above room temperature [7,8]. BFO has a ferroelectric Curie temperature T_c of 850 °C and an antiferromagnetic Néel temperature of 370 °C [5,8-11]. BFO based systems may be used to develop novel applications in the field of memory devices, radio, sensors, television, microwave and satellite communication, audio-video and digital recording, optical filters and smart devices, etc. [9,11-13].

Recently, researchers have attempted to prepare phase pure BFO via a variety of routes, such as conventional solid-state reaction [14,15], co-precipitation [16,17], soft chemical route [15,18], ferrioxalate precursor method [19,20], microemulsion technique [21], hydrothermal route [16,22-26] and sol-gel process [18,27,28], have been developed to synthesize BFO micrometer and nanometer sized crystallites [29,30]. Among these methods, the Hydrothermal method has been used due to its simple, energy saving, cost effective and allowing the control of grain size, morphology and crystallinity by easy changes in the experimental details [31,32].

In the present experimental work, bismuth ferrite nanocomposites were prepared by using the hydrothermal method at low temperature. The phase structure evolution of BFO under designated hydrothermal conditions was investigated and discussed.

1. Experimental

1.1. Preparation of Graphene Oxide

Graphene oxide was prepared by a modified Hummers method. In this method, 1 g graphite powder, 0.5 g sodium nitrate and 23 ml sulfuric acid were mixed into a beaker and exposed stirring for 30 min in an ice bath. Then 3 g potassium permanganate was slowly added to mixture solution by magnetic stirring through 6 hours. Subsequently, after the solution was kept in the ultrasonic machine for 2 hours and 100 ml distilled water and 2ml H_2O_2 (30%) were added by using a magnetic stirrer. Finally, the solution was washed with de-ionized water and filtered until pH value reached to 7.

1.2. Synthesis of The Nanopowders

The chemical reagents used in the present work were bismuth nitrate ($BiNO_4$), Iron(III) Chloride Hexahydrate ($FeCl_3.6H_2O$) and potassium hydroxide (KOH) as mineralizer and deionized water as a reaction medium. All chemicals source are analytical grade. Firstly, $BiNO_4$ and then $FeCl_3.6H_2O$ were added to the solution. The solutions were stirred at room temperature for 2 h to obtain a homogeneous solution. Then, KOH was slowly added to the above Fe-Bi solution to coprecipitate. The precipitate was mixed with KOH under constant magnetic stirring for 30 min. After, Graphene oxide solution was added to the solution. The suspension solution was poured into a teflon lined stainless steel autoclave for the hydrothermal process. The process was carried out for 6 h at temperature of 200 °C. After the hydrothermal reaction, the autoclave was cooled naturally to room temperature. The products were

filtered and washed with de-ionized water in sequence to remove all soluble salts and then dried at room temperature for 24 h.

1.3. Characterization

XRD patterns of obtained nanopowders were characterized using a BRUKER ADVANCE D8 X-Ray Diffractometer with Cu Kα radiation (λ = 1.5406 Å) in the 2θ range from 20 to 80° with 0.02 °/min. X-ray diffraction spectra of all the samples were taken at room temperature. The morphology and structural properties of nano electroceramics were investigated using a High-Resolution scanning electron microscope (JEOL JEM-2100F SEM). High-Resolution Transmission Electron Microscopy (JEOL 2001 HRTEM) was done at an accelerating voltage of 200KV to confirm the microstructure. The optical spectra of the samples were performed using a SHIMADZU UV–VIS–NIR 3600 model spectrophotometer in the wavelength range of 200–1400 nm at room temperature. Thermogravimetric analysis (TGA) and differential thermal analysis (DTA) (SHIMADZU DTG-60AH) of BFO powders was carried out from room temperature to 900 °C in Argon ambient at a scan rate of 10 °C/min. FTIR spectra studies were made with Thermo Scientific Nicolet IS5 mark Fourier transform infrared spectrometer with an ID5 ATR sample holder. The dielectric and alternating current conductivity properties were investigated using a HIOKI 3532-50 LCR HITESTER at room temperature.

2. Results and Discussions

The X-ray diffraction patterns (XRD) of the synthesized Bismuth Ferrite nanopowder prepared by hydrothermal route are shown in Figure 1. XRD pattern of the samples were appeared at 2θ values 24.204°, 36.609° and 49.542° corresponding to (220), (411) and (211) reflections, respectively. The observed all peaks in Figure 1 can be indexed to the $Bi_{46}Fe_2O_{72}$ polycrystalline structure with the cubic structure according to (JCPDS 00-020-0170) with the lattice constants: *a* = 10,191 nm and space group *Pbam* at room temperature. As seen in the XRD peaks, the intensity of peaks is changed with increasing Graphene oxide doping. This indicates that Graphene oxide is incorporated into sites of $Bi_{46}Fe_2O_{72}$. The crystallite size of the Bismuth Ferrite nanoceramics were calculated from the Debye–Scherrer formula[33,34].

$$D = \frac{0.9\,\lambda}{\beta.cos\theta} \tag{1}$$

where λ is the X-ray wavelength (1,5406 Å), θ is the Bragg diffraction angle and β is the full width at half-maximum of the main peak in the XRD pattern. The calculated values of the crystallite sizes for BFO/Graphene oxide ceramic prepared via hydrothermal process are given in Table 1. The calculated crystallite sizes are changed when Graphene Oxide doping were varied from 0 to 100 mg (As seen Table 1). The lattice constant *a* was obtained from interplaner spacing of d_{hkl} value of the (2 2 0) and (4 1 1) peaks using the following equation [33,34]:

$$d_{h\,k\,l} = \frac{a}{\sqrt{h^2+k^2+l^2}} \tag{2}$$

Where *a* is the lattice parameter, h,k,l is the miller indices and d_{hkl} is the interplanar distance for the atoms. The lattice parameter of the nanocomposites were determined and are given in **Table 1.** The lattice parameters of the samples did not significantly changed with graphene oxide doping.

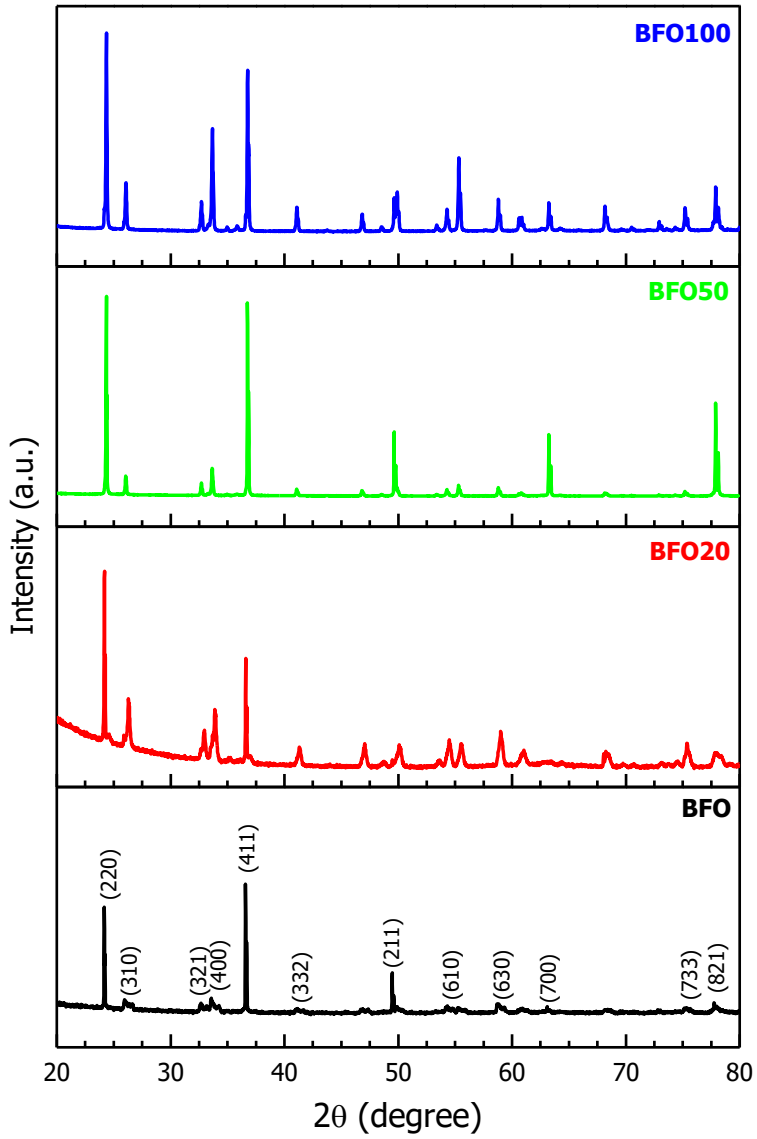

Figure 1. XRD patterns of BFO/GO nanopowders

Table 1. X-Ray diffraction parameters of Bismuth Ferrite/Graphene oxide nanoceramics

	2 θ (°)	h	k	l	*a*	d (Å)	FWHM	D (nm)
BFO	24.204	2	2	0	10.191	3.67415	0.101	82.89
	36.609	4	1	1		2.45267		
BFO20	24.202	2	2	0	10.191	3.67448	0.076	106.95
	36.661	4	1	1		2.44930		
BFO50	24.355	2	2	0	10.191	3.65175	0.078	104.24
	36.778	4	1	1		2.44178		

BFO100	24.353	2	2	0	10.191	3.65201	0.107	75.99
	36.796	4	1	1		2.44062		

SEM photographs and EDX analysis of pure and graphene oxide modified bismuth ferrite nanopowders prepared by hydrothermal methods are shown in Figure 2 (a,b,c,d).The photographs reveals that the grains are non-uniform, agglomered and less densified with interconnected structure. The average grain size for BF0, BFO20, BFO50 and BFO100 was found to be 351, 337, 411 and 371nm, respectively. The powders are formed from the nanoparticles and their size is changed with graphene oxide doping.

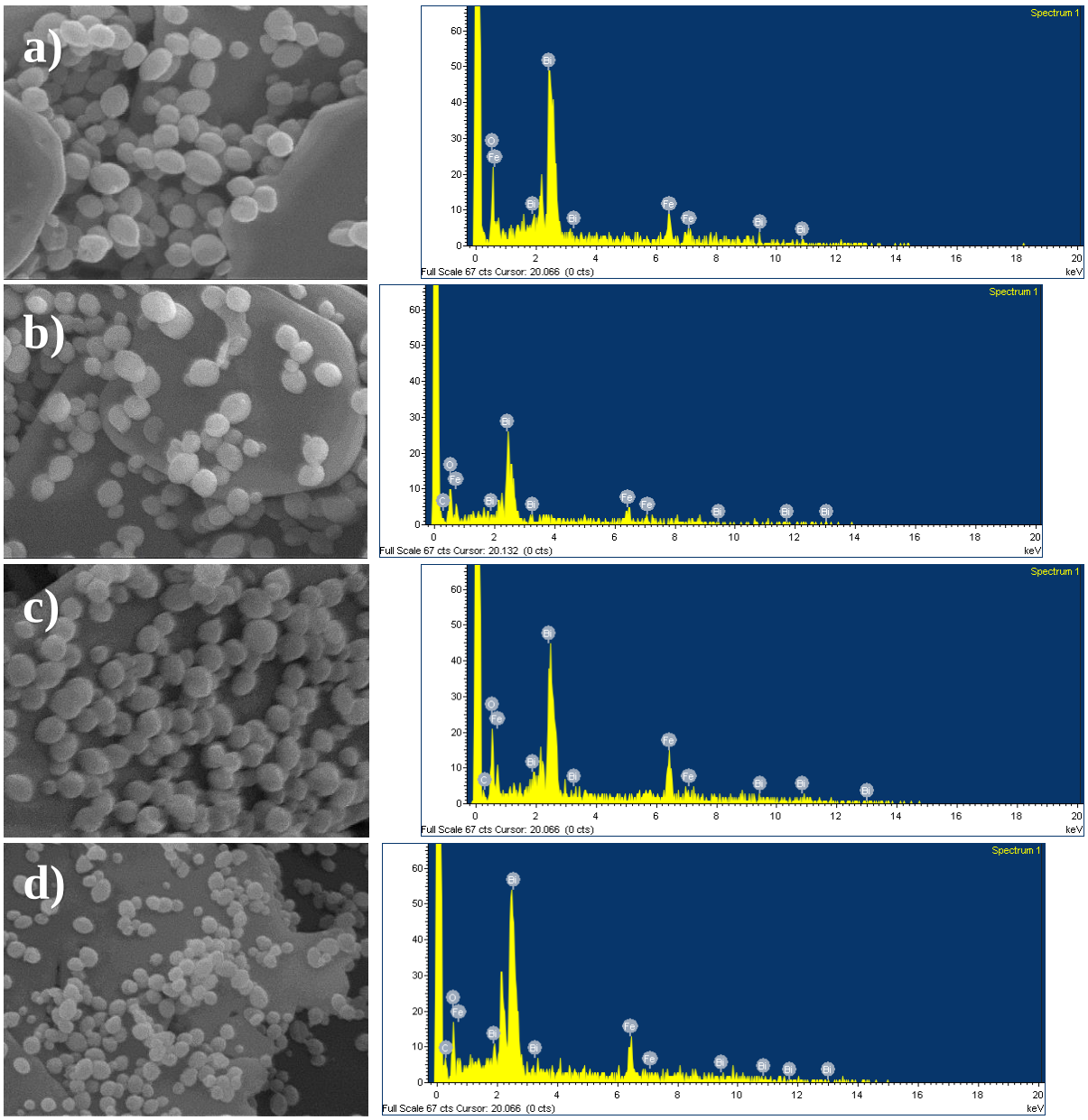

Figure 2: SEM photographs and EDX of the synthesized nanoelectroceramics (20.000X) a) BFO b) BFO20 c) BFO50 and d) BFO100

HR-TEM images and selected area electron diffraction (SAED) images of the synthesized bismuth ferrite nanoceramics. are shown in Figure 3. (a, b, c, d). It was perceived that most of the

particles had spherical shape. From SAED image it is clear that the particles are well crystalline in case of the hydrothermal process.

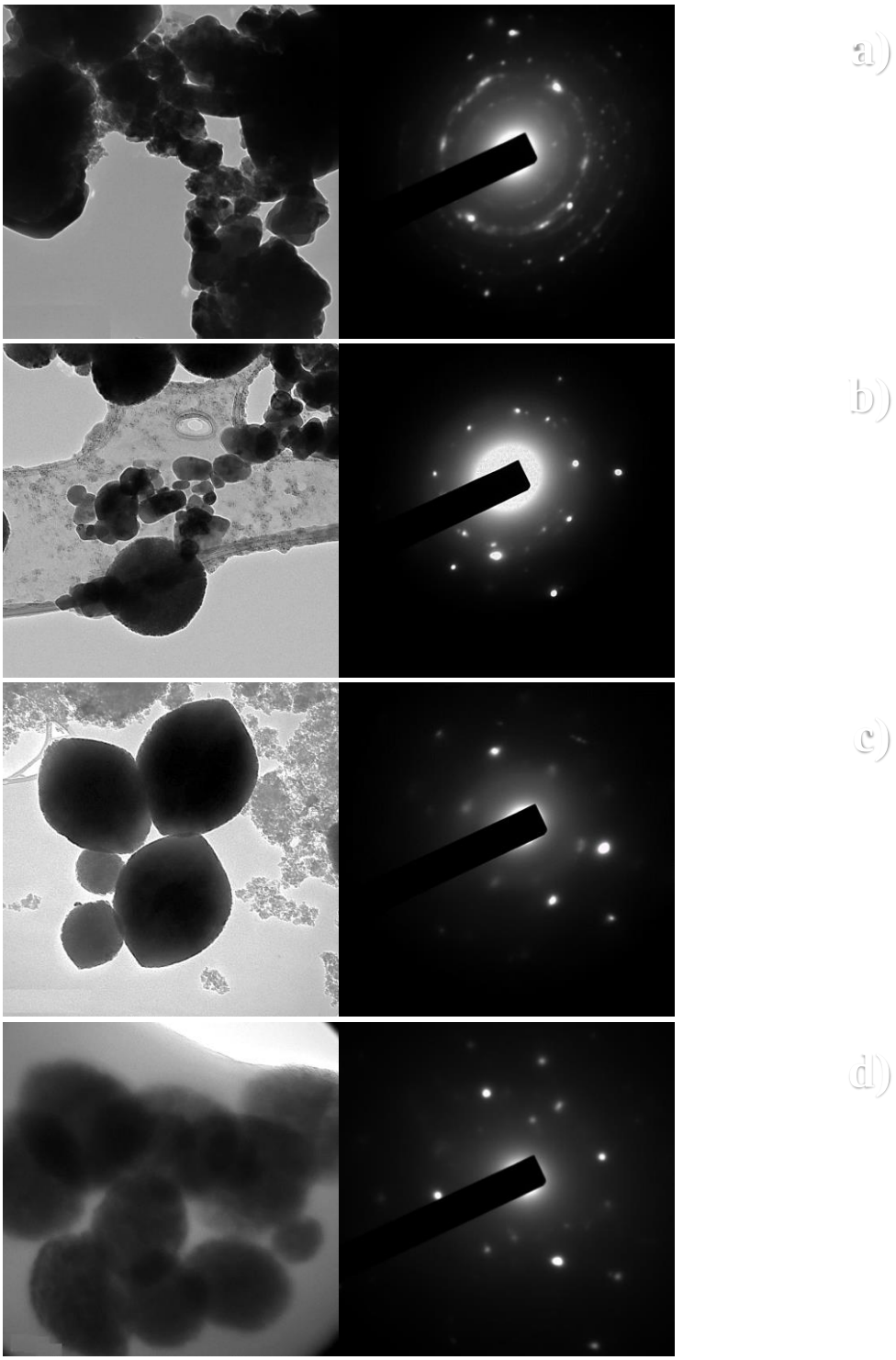

Figure 3. HRTEM image and SAED pattern of the samples a) BFO b) BFO20 c) BFO50 and d) BFO100

Thermogravimetric analysis (TGA) and differential thermal analysis (DTA) curves of bismuth ferrite nanoceramics are shown in Figure 4.(a, b, c, d). The DTA/TGA curve depicts a weight loss up to 900 °C, which is due to the presence of trapped nitrates, residual chlorite and entrapped water.

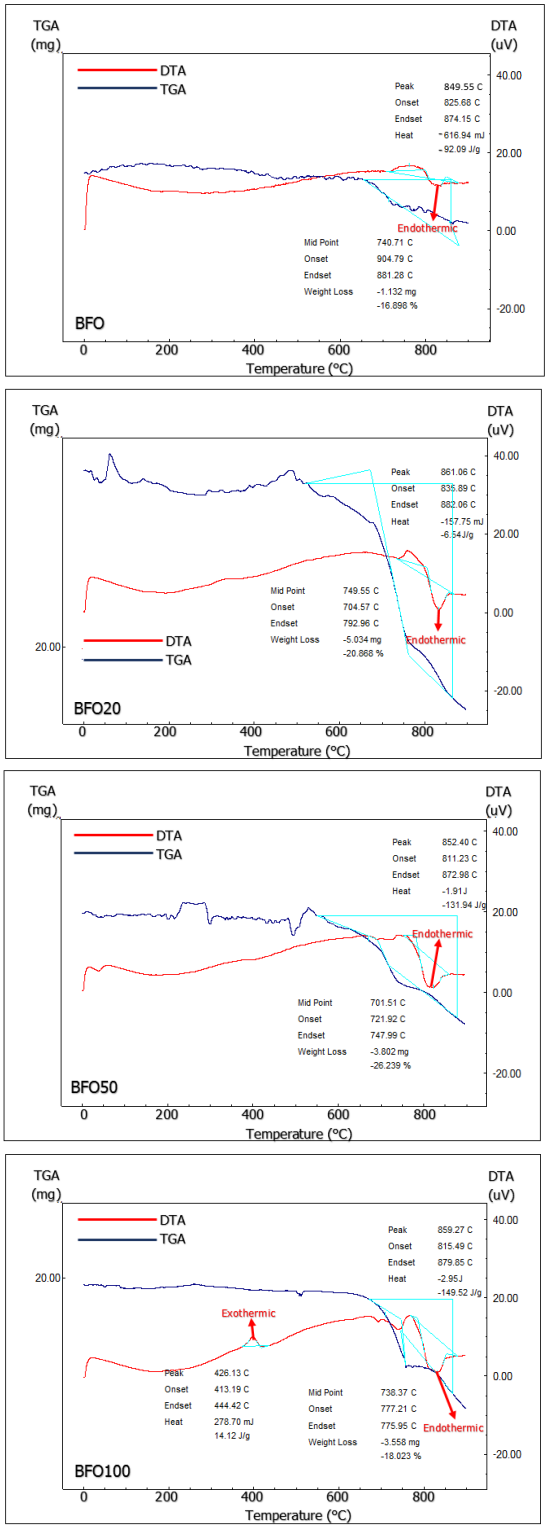

Figure 4: DTA /TGA curves of the nanopowders a) BFO b) BFO20 c) BFO50 and d) BFO100

The FT-IR spectra of crystalline nano bismuth ferrite powders derived from the hydrothermal reaction for different graphene oxide quantity are shown in Figure 5. The broadband at 3000–3600cm^{-1} arose from the antisymmetric and symmetric stretching of bond H_2O and OH^- groups, while a band at 1607cm^{-1} corresponded to the bending vibrations of H_2O. The sharp band around 2360 cm−1 suggested that atmospheric carbon dioxide exists in the sample. The band at around 1339cm^{-1} was due to the presence of trapped nitrates. Specifically, the strong absorptive peaks at 590cm^{-1} was attributed to the

Fe–O stretching and bending vibration, being characteristics of the octahedral FeO_6 groups in the compounds. The formation of perovskite structure can be confirmed by the presence of metal-oxygen band [10,13,16,32,35,36].

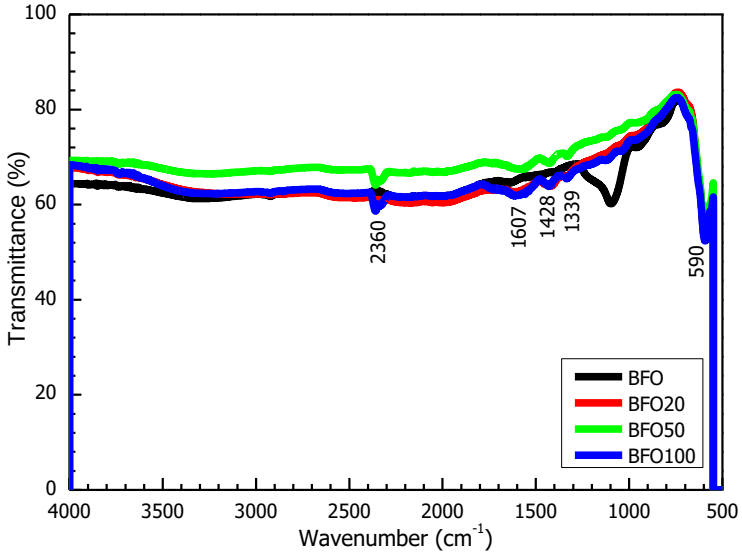

Figure 5: FT-IR spectra of BFO/Graphene oxide nanocomposite

The dielectric properties of BFO/GO nano electroceramics (real and imaginer) with respect to frequency variation (1KHz–2MHz) was measured with the LCR analysis at room temperature. Using the following relations, the relative permittivity (ε'), dielectric loss (ε'') and alternating current conductivity (σ_{ac}) values of the samples were estimated [37]:

$$\varepsilon' = \frac{C\,.\,l}{\varepsilon_0\,.A} \tag{3}$$

$$\varepsilon'' = \tan\delta\,.\,\varepsilon' \tag{4}$$

$$\sigma_{ac} = \frac{l}{Z\,.\,A} \tag{5}$$

where ε_0 is the permittivity of free space, A is the area of the electrode and C and l are the capacitance and thickness of the sample, respectively. tanδ is the loss tangent and Z is the impedance. The relative permittivity (ε'), often called the dielectric constant, versus frequency of samples are presented in Fig.6. It is show that ε' change with increasing frequency. The ε' values of the samples at 1 kHz are found to be 6.415, 6.796, 6.110 and 3,426 for BFO, BFO20, BFO50 and BFO100, respectively. As it is well known, the induced electric dipoles cause the formation of polarization. Therefore, the change in the relative permittivity values could be explained by polarization mechanism, and ionic polarization was responsible for this change.

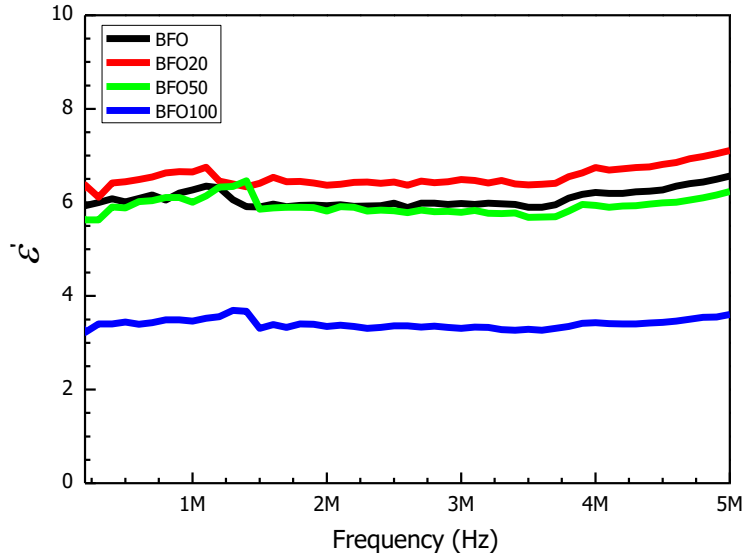

Figure 6: Frequency dependence of real part of dielectric constant (ε') at room temperature.

Fig.7 shows variation of dielectric loss (ε'') versus frequency obtained for bismuth ferrite samples at room temperature shows the dielectric loss changes with increasing frequency.

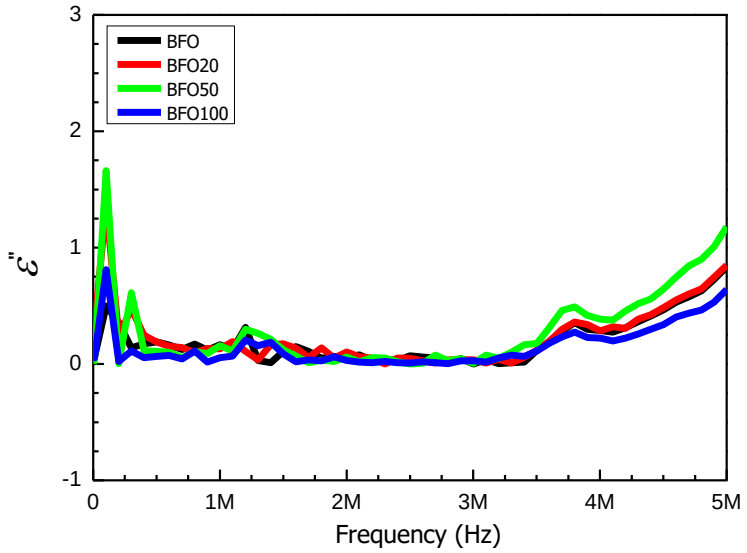

Figure 7: The frequency (f) dependence of the dielectric loss (ε'') of nanocomposites.

As seen in Fig. 8, the *AC* conductivity for all the investigated samples increases almost linearly with increasing frequency. This suggests that the frequency of the applied field is lower than the charge carrier jump frequency in the solid.

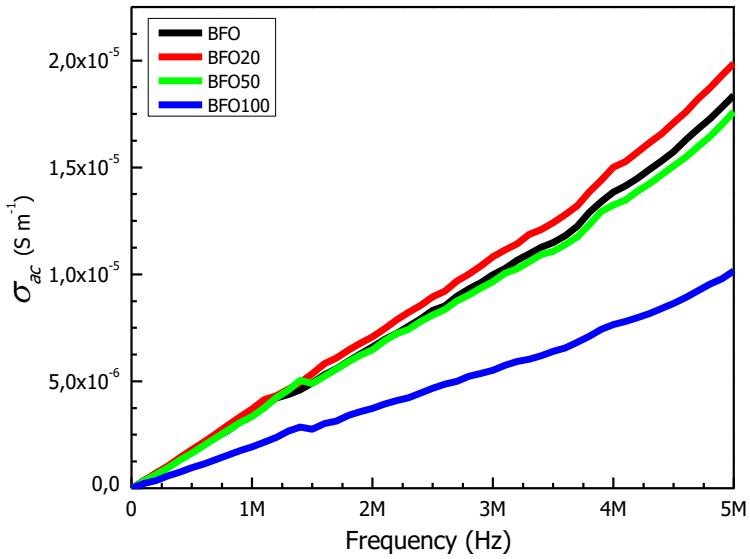

Figure 8: The alternating current conductivity as a function of frequency

Fig.9. shows the room temperature *P-E* hysteresis loop of all BFO/GO samples. The loop shows proper saturation with enhanced saturation polarization (Ps), remnant polarization (Pr) and coercive electric field (Ec).

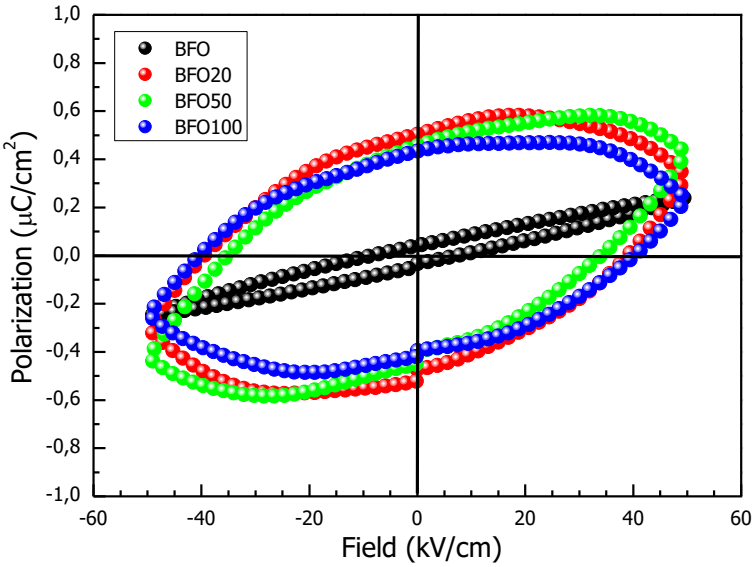

Figure 9: P-E Hysteresis loop of BFO/GO nanoceramics

Table 2. Maximum polarization (P_{max}), remnant polarization (P_r) and coercive electric field (E_c) of Bismuth ferrite/Graphene oxide nano electroceramics.

	P_{max} (μC/cm^2)	**P_r (μC/cm^2)**	**E_c (kV/cm)**
BFO	0,203	0,0384	8,460
BFO20	0,152	0,471	17,071

BFO50	0,022	0,406	22,181
BFO100	0,160	0,402	37,654

Electrical conductivity reveals reliable information about the transport phenomenon of samples. The electrical transport mechanisms of BFO/GO nanomaterials were investigated by the temperature dependent conductivity as seen in Fig. 10. The electrical conductivity changes with increasing temperature of all samples. E_A values of the nanocomposites did not show a regular trend with increasing graphene oxide content This is due to the non-uniform distribution of graphene oxide into Bismuth ferrite host matrix. The composite with BFO exhibits the lowest activation energy, whereas the highest activation energy was found to be for BFO50. All the curves can be separated into one linear regions. The electrical conductivity can be all analyzed by Arrhenius's equation [38-41]:

$$\sigma_{dc} = \sigma_0 \,.\exp\left(\frac{\Delta E_A}{kT}\right) \tag{6}$$

where σ_0 is the pre-exponential factor, k is the Boltzmann's constant and ΔE_A is the activation energy for the conductivity. Table 2 demonstrates the ΔE_A values calculated from the linear portions of curves in Fig. 11. The electrical conductivity results indicate that the electrical conduction mechanism is thermally activated process and *dc* conductivity increases exponentially over the studied range of temperatures. The electrical conductivity of the Bismuth Ferrite increases with increasing graphene oxide dopants.

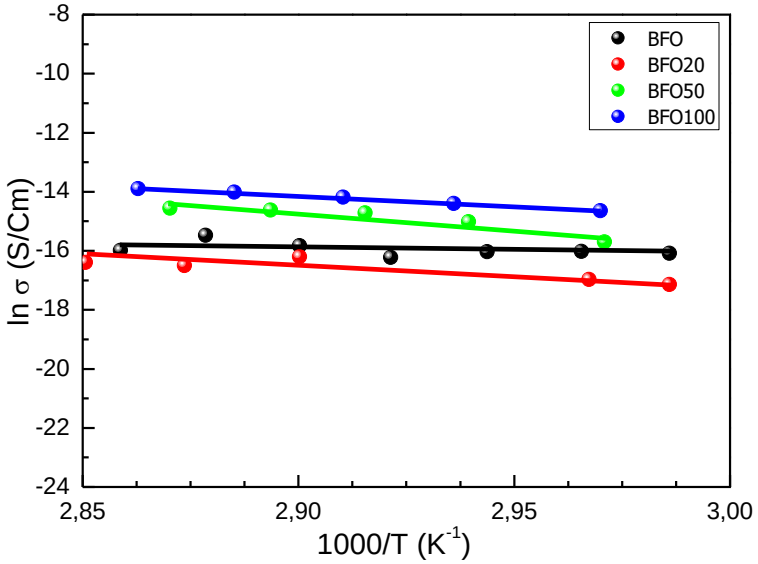

Figure 10: Temperature dependent of the electrical conductivity of BFO/GO nanocomposites

To determine the optical band gap of Bismuth ferrite/Graphene oxide nanostructures, the reflectance spectra of the powder samples were measured as shown in Fig. 11. As seen in Fig. 11, the reflectance of the samples increases with increasing the wavelengths.

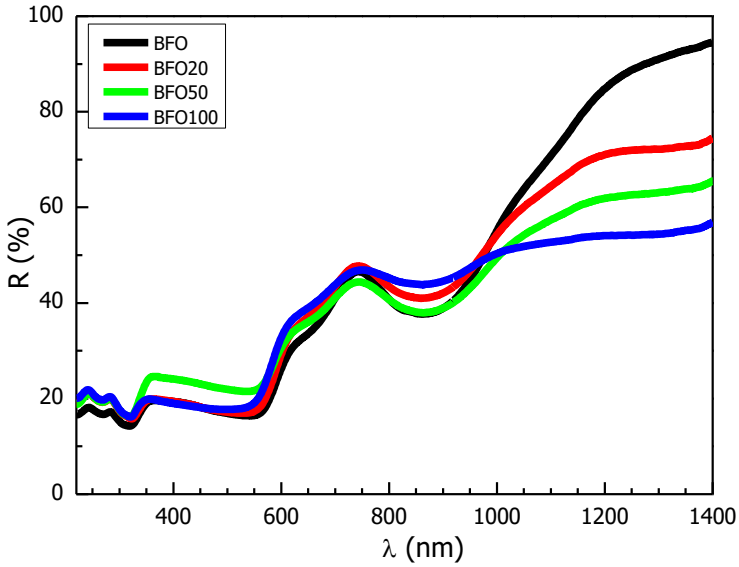

Figure 11: The reflectance spectra of the undoped and Graphene oxide doped BFO nanoceramics

In order to determine the precise value of optical band gap of pure and graphene oxide-doped BFO nanostructures, the reflectance values were converted to absorbance by application of the Kubelka–Munk function [25–27]. It provides a correlation between reflectance and concentration. The concentration of an absorbing species can be determined using the Kubelka–Munk formula [33,38, 42]:

$$F(R) = \frac{(1-R)^2}{2R} \tag{6}$$

where R is the diffused reflectance. F(R) is Kubelka–Munk function which corresponds to the absorbance. Optical spectroscopy is developed as an important experimental tool for the determination of energy band of materials. Optical characterization of nanocomposites was carried out by measuring the reflectance spectroscopy at room temperature. The fundamental absorption, which corresponds to electron excitation from the valence band to conduction band, can be used to determine the value of the optical band gap E_g and it is related to the optical transition. The relation between the absorption coefficient ˛ and the incident photon energy h can be written as The optical band gap of samples can be then determined by the following relation [43-46]:

$$\alpha h\nu = A\,.\,(h\nu - E_g)^n \tag{7}$$

where A is a constant depending on the transition probability and n is an index that characterizes the optical absorption process. The parameter n has the value 1/2 for the direct allowed transition and has the value 2 for the indirect allowed transition.

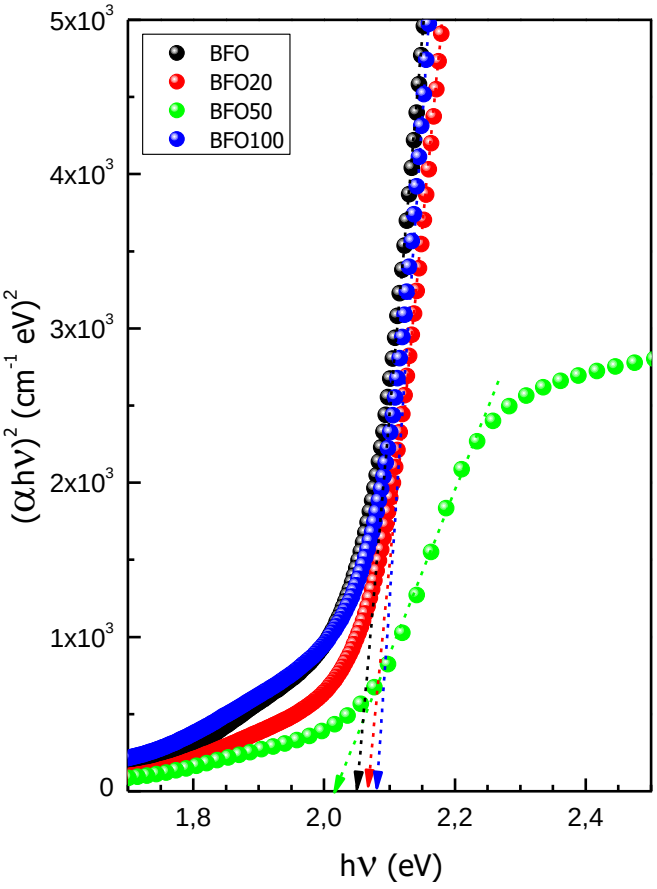

Figure 12: The plots of $(\alpha h\upsilon)^2$ vs. photon energy of the BFO/GO nanoceramics

Table 3. Optical band gap (E_g)and the electrical activation energy (ΔE_A) of Bismuth ferrite/Graphene oxide nanopowders.

	Optical Bandgap	**Activation Energy**	**Conductivity**
	E_g (eV)	(ΔE_A) (eV)	σ_{dc} (S/cm) at 303 K
BFO	2.051	0,327	$7{,}24\times10^{-8}$
BFO20	2.064	0,411	$9{,}41\times10^{-9}$
BFO50	2.025	0,996	$3{,}51\times10^{-8}$
BFO100	2.089	0,618	$5{,}53\times10^{-8}$

3. Conclusions

We have successfully synthesized the phase pure multiferroic nanopowders of BFO by the low-temperature hydrothermal method. XRD data confirms that the hydrothermal synthesized BFO/GO ceramic nanocomposites in the cubic structure. The X-ray patterns suggest that BFO crystallite size varying from 75.99 nm to 106.95 nm. The ferroelectric measurement reveals the ferroelectric nature of BFO/GO with saturation. The room temperature dielectric measurement with frequency reveals the dielectric constant and loss increases with increasing frequency for samples. The resistivity is change

with graphene oxide concentration and follows the Arrhenius behavior. The activation energy was found to be 0.327, 0.411, 0,996 and 0,618 eV for BF0, BFO20, BFO50 and samples, respectively. Optical band gap was observed to vary from 2.051 eV to 2.025 eV. Diffuse reflectance spectroscopy measurements of nano electroceramics indicate that band gap changed with the change in particle size.

Acknowledgements

This work was supported by the Management Unit of Scientific Research Projects of Firat University (FUBAP) (Project Number: FF.16.29). Authors thank to Firat University for supporting.

4. References

[1] Sakar M., Balakumar S., Saravanan P., Jaisankar S.N., *Mater Res Bull*, 48 (2013), 2878-2885.
[2] Mukherjee S., Mitra M. K., *J Aust Ceram Soc*, 50 [2] (2014), 180-187.
[3] Wang Y., Xu G., Yang L., Ren Z., Wei X., Weng W., Du P., Shen G., Han G., *J Am Ceram Soc*, 90 [11] (2007), 3673-3675.
[4] Yang X., Zhang Y., Xu G., Wei X., Ren Z., Shen G., Han G., *Mater Res Bull*, 48 (2013), 1694-1699.
[5] Chen C., Cheng J., Yu S., Che L., Meng Z., *J Cryst Growth*, 291 (2006),135-139.
[6] Gao T., . Chen Z, Huang Q., Niu F., Huang X., Qin L., . Huang Y, *Rev Adv Mater Sci*, 40 (2015), 97-109.
[7] Zhang H., Kajiyoshi K., *J Am Ceram Soc*, 93 [11] (2010), 3842-3849.
[8] Chen X-Z., Qiu Z-C., Zhou J-P., Zhu G., Bian X-B, Liu P., *Mater Chem Phys*, 126 (2011), 560-567.
[9] Chen C., Cheng J., Yu S., Che L., Meng Z., *J Cryst Growth*, 291 (2006), 135-139.
[10] Aguiara E.C., Ramirez M.A., Moura F., Varelaa J.A., Longoa E., Simoes A.Z., *Ceram Int*, 39 (2013),13-20.
[11] Srivastav S. K., Gajbhiye N. S., *J Am Ceram Soc*, 95 [11] (2012), 3678-3682.
[12] Ghosh S., Dasgupta S., Sen A., Maiti H. S., *Mater Res Bull*, 40 (2005), 2073-2079.
[13] Biasotto G., Simo A.Z., Foschini C.R., Zaghete M.A., Varela J.A., Longo E., *Mater Res Bull* , 46 (2011), 2543-2547.
[14] Achenbach G.D., James W.J., Gerson R., *J Am Ceram Soc*, 8 (1967), 437-438.
[15] Sakar M., Balakumar S., Saravanan P., Jaisankar S.N., *Mater Res Bull*, 48 (2013), 2878-2885.
[16] Xu J-H., Ke H., Jia D-C., Wang W., Zhou Y., *J Alloy Compd*, 472 (2009), 473-477.
[17] Shetty S., Palkar V.R., Pinto R., Pramana, *J Phys*, 58 (2002), 1027-1030.
[18] Ghosh S., Dasgupta S., Sen A., Maiti H.S., *J Am Ceram Soc*, 88(5) (2005), 1349-1352.
[19] Ghosh S., Dasgupta S., Sen A., Maiti H.S., *Mater Res Bull*, 40 (2005), 2073-2079.
[20] Ghosh S., Dasgupta S., Sen A., Maiti H. S., *P Mater Res Bull*, 40 [12] (2005), 2073–9
[21] Das N., Majumdar R., Sen A., Maiti H.S., *Mater Lett*, 61 (10) (2007), 2100-2104.
[22] Chen C., Cheng J., Yu S., Che L.J., Meng Z.Y., *J Cryst Growth*, 291 (2006), 135-139.
[23] Han J.T., Huang Y.H., Wu X.J., Wu C.L., Wei W., Peng B., Huang W., Goodenough J.B., *Adv Mater*, 18 (2006), 2145-2148.
[24] Xiaomeng L., Jimin X., Yuanzhi S., Jiamin L., *J Mater Sci*, 42 (2007), 6824-6827.
[25] Wang Y., Xu G., Ren Z., Wei X., Weng W., Du P., Shen G., Han G., *J Am Ceram Soc*, 90 (2007), 2615-2617.
[26] C Cho.M., Noh J.H., Cho İ.-S., An J.-S., Hong K.S., Kim J.Y., *J Am Ceram Soc*, 91 (2008), 3753-3755.
[27] Kim J.K., Kim S.S., Kim W.J., *Mater Lett*, 59 (2005), 4006-4009.

[28] Park T.J., Papaefthymiou G.C., Viescas A.J., Moodenbaugh A.R., Wong S.S., *Nano Lett*, 7 (2007), 766-772.
[29] Wang Y., Xu G., Yang L., Ren Z., Wei X., Weng W., Du P., Shen G., Han G., *Ceram Int*, 35 (2009), 1285-1287.
[30] Han S. H., Kim K. S., Kim H. G., Lee H.-G., Kang H.-W., Kim J. S., Cheon C. I., *Ceram Int*, 36 (2010), 1365-1372.
[31] Fruth V., Mitoserıu L., Berger D., Ianculescu A., Matei C., Preda S., Zaharescu M., *Prog Solid State Ch*, 35 (2007), 193-202.
[32] Chen C., Cheng J., Yu S., Che L., Meng Z., *J Cryst Growth*, 291 (2006), 135-139.
[33] Aydin C., El-Nasser H.M., Yakuphanoglu F., Yahia I.S., Aksoy M., *J Alloy Compd*, 509 (2011), 854-858.
[34] Aydin C., Al-Hartomy Omar A., Al-Ghamdi A. A., Al-Hazmi F., Yahia I. S., El-Tantawy F., Yakuphanoglu F., *J Electroceram*, 29(2012), 155-162.
[35] Slamovich E.B., Aksay I.A., *J Am Ceram Soc*, 79 (1996), 239.
[36] Li S., Condrate Sr R.A., Jang S.D., Spriggs R.M., *J Mater Sci*, 24 (1989), 3873.
[37] Kaygili O., Keser S., Ates T., Kirbag S., Yakuphanoglu F., *Mater Sci*, 22 (2016), 1392-1320.
[38] Aydin C., Abd El-Sadek M.S., Zheng K., Yahia I.S., Yakuphanoglu F., *Opt Laser Technol*, 48 (2013), 447-452.
[39] Aydin C., Benhaliliba M., Al-Ghamdi A. A., Gafer Z. H., El-Tantawy F., Yakuphanoglu F., *J Electroceram*, 31 (2013), 265-270.
[40] Guler O., Guler S. H., Yakuphanoglu F., Aydin H., Aydin C., El-Tantawy F., Duraia El-Shazly M., Fouda A. N., *Fuller Nanotub Car N*, 23 (2014), 865-869.
[41] Aydin C., Khusayfan N. M., Al-Ghamdi Ahmed A., El-Tantawy F., Farooq W. A., Yakuphanoglu F., *J Sol-Gel Sci Technol*, 78 (2016), 68.
[42] Aydin C., Al-Hartomy Omar A., Al-Ghamdi A. A., Al-Hazmi F., Yahia I. S., El-Tantawy F., Yakuphanoglu F., *J Electroceram*, 29 (2012), 155-162.
[43] Aydin H., Mansour Sh. A., Aydin C., A. Al-Ghamdi A., Al-Hartomy O.A., El-Tantawy F., Yakuphanoglu F., *J Sol-Gel Sci Technol* 64 (2012), 728-733.
[44] Aydin C., Mansour Sh. A., Alahmed Z. A., Yakuphanoglu F., *J Sol-Gel Sci Technol*, 62 (2012), 397-403.
[45] Aydin H., Tataroglu A., Al-Ghamdi A. A., Yakuphanoglu F., El-Tantawy F., Farooq W.A., *J Alloy Compd*, 625 (2015), 18-25.
[46] Aydin H., El-Nasser H.M., Aydin C., Al-Ghamdi A. A., Yakuphanoglu F., *Appl Surf Sci*, 350 (2015), 109-114.